https://doi.org/10.5194/hess-2020-429
Preprint. Discussion started: 8 October 2020
© Author(s) 2020. CC BY 4.0 License.

Hydrology and Earth System Sciences
Open Access
EGU
Discussions

The evolution of stable silicon isotopes in a coastal carbonate aquifer, Rottnest Island, Western Australia

Ashley N. Martin[1,2,3,4,*], Karina Meredith[1,2,] , Andy Baker[1,3] Marc D. Norman[5] and Eliza Bryan[1,2,3]

[1]Connected Waters Initiative Research Centre, UNSW Sydney, Sydney, NSW 2052, Australia.

[2]Australian Nuclear Science and Technology Organisation, Lucas Heights, NSW 2234, Australia.

[3]School of Biological, Earth and Environmental Sciences, UNSW Sydney, Sydney, NSW 2052, Australia.

[4]Institut für Mineralogie, Leibniz Universität Hannover, Callinstraße 3, 30167 Hannover, Germany.

[5]Research School of Earth Sciences, Australian National University, Canberra, ACT 2601, Australia.

**Correspondence to*: a.martin@mineralogie.uni-hannover.de

Abstract. Dissolved silicon (DSi) is a key nutrient in the oceans, but there are few data available regarding Si isotopes in coastal aquifers. Here we investigate the Si isotopic composition of 12 fresh and 17 saline groundwater samples from Rottnest Island, Western Australia, which forms part of the world's most extensive aeolianite deposit (the Tamala Limestone Formation). Two bedrock samples were also collected from Rottnest Island for Si isotope analysis. The δ^{30}Si values of groundwaters ranged from -0.39 to +3.60 ‰ with an (average: +1.59 ‰) and the rock samples were -0.76 and -0.13 ‰. Due to the relatively low concentrations of DSi (64 to 196 µM) and clay-forming cations in fresh groundwaters, the correlation between δ^{30}Si values and DSi concentrations (ρ = 0.59, p = 0.02) may be explained by Si adsorption onto Fe-Al (oxy)hydroxides present in the aquifer. An increase in groundwater δ^{30}Si in association with the occurrence of water-rock interactions may explain the spatial pattern in δ^{30}Si across the aquifer, and is consistent with the correlation between δ^{30}Si and tritium activities when considering all groundwaters (ρ = -0.68, p = 0.0002). In the deeper aquifer, the inverse correlation between DSi and Cl concentrations (ρ = -0.79, p = 0.04) for the more saline groundwaters is attributed to groundwater mixing with local seawater that is depleted in DSi (<3.6 µM). Our results from this well-constrained, island aquifer system demonstrate that stable Si isotopes usefully reflect the degree of water-rock interactions, which is related to groundwater residence time and local hydrogeology. Our finding that lithogenic Si dissolution occurs in the freshwater lens and the freshwater-seawater transition zone on Rottnest Island appears to supports the recent inclusion of a marine submarine groundwater discharge term in the global DSi mass balance. Finally, geologically-young, carbonate aquifers, such as Rottnest Island, may be an important source of DSi in coastal regions with low riverine input and low oceanic DSi concentrations.

1. Introduction

Dissolved silicon ($Si(OH)_4$; DSi) is a key nutrient in global biogeochemical cycles that is sourced primarily from continental silicate weathering (Tréguer et al., 1995;Tréguer and De La Rocha, 2013;Rahman et al., 2017;Rahman et al., 2019;Frings et al., 2016). Thus, the DSi flux from the continents is a key control on primary productivity in the global biogeochemical cycles of the oceans (Falkowski et al., 1998). Stable silicon isotopes (^{28}Si, ^{29}Si and ^{30}Si) are useful for tracing the rate and extent of silicate weathering reactions due to the preferential incorporation of lighter Si isotopes into during clay mineral formation (Frings et al., 2015;Pogge von Strandmann et al., 2012;Hughes et al., 2013;Georg et al., 2009a;Georg et al., 2007), silica precipitation (Geilert et al., 2014;Oelze et al., 2015), and adsorption of Si onto Fe-Al (oxy)hydroxides (Opfergelt et al., 2009;Opfergelt et al., 2017). Biological processes also fractionate Si isotopes as DSi is utilised by organisms such as diatoms and vascular plants (Ding et al.,

https://doi.org/10.5194/hess-2020-429
Preprint. Discussion started: 8 October 2020
© Author(s) 2020. CC BY 4.0 License.

2008;De La Rocha et al., 1998;Meyerink et al., 2017). Moreover, Si isotopes are not fractionated during congruent mineral dissolution and there is a narrow range of ^{30}Si values for the upper continental crust (UCC): -0.25 ± 0.16 ‰ (2 standard deviations (s.d.); Savage et al., 2013). Therefore, DSi isotopic ratios may reflect the balance between congruent silicate dissolution and secondary mineral formation such that if the global Si budget is well constrained, marine Si isotope records may be used to reconstruct past changes in continental weathering and primary productivity (Frings et al., 2016;De La Rocha et al., 1998;Christina et al., 2000).

The global DSi isotopic budget is poorly constrained for groundwater systems (Frings et al., 2016), despite around half of the total dissolved solids (TDS) flux to the oceans deriving from submarine groundwater discharge (SGD) (Zektser and Loaiciga, 1993). Globally, average dissolved δ^{30}Si values in low-temperature groundwater systems (+0.19 ± 0.81 ‰) are lower than those in rivers (+1.25 ± 0.68 ‰; 1 s.d.; Frings et al., 2016). The lower δ^{30}Si values in some groundwater systems may be due to the greater extent of water-rock interactions compared to surface waters and the dissolution of ^{30}Si-depleted secondary minerals (Basile-Doelsch et al., 2005;Georg et al., 2009b;Pogge von Strandmann et al., 2014). The δ^{30}Si values reported for groundwater DSi are highly variable even within a single system, e.g., ranging from −0.15 to +1.34 ‰ at various depths in the alluvial Bengal Basin aquifer in India (Georg et al., 2009a), +0.35 to +1.01 ‰ for volcanic springs in Iceland (Opfergelt et al., 2011), −1.42 to +0.56 ‰ in a sandstone aquifer in Arizona, U.S. (Georg et al., 2009b), and −1.50 to −0.85 ‰ in the sedimentary Great Artesian Basin, Australia (Pogge von Strandmann et al., 2014). Although ~12% of the global SGD flux flows through carbonate aquifers (Beck et al., 2013), these systems have received little attention thus far. This is because carbonates are not expected to contain much Si; however, some carbonate-dominated aquifers contain copious amounts of silica-bearing material of various origins, e.g., alluvial, aeolian, pedogenic, etc. (Muhs, 2017).

Here we present Si isotopic compositions of groundwater from a coastal carbonate aquifer, Rottnest Island (RI), Australia. There is a freshwater lens on RI located above a ~10 m freshwater-seawater transition zone (Playford et al., 1977). Conventional stable isotope data (^{2}H, ^{13}C, and ^{18}O), tritium (^{3}H) and radiocarbon (^{14}C) measurements show that the freshwater lens aquifer on RI is recharged by modern rainfall, which fluctuates due to climatic variations, and that the residence time for fresh groundwaters ranges from ~12 to 36 years (Bryan et al., 2020). The stable isotope and major element (Mg, Ca) geochemistry of fresh RI groundwaters is dominated by carbonate weathering reactions (Bryan et al., 2017). These reactions are not expected to affect groundwater δ^{30}Si values due to the low Si incorporation into the carbonate minerals, e.g. the DSi partition coefficient for precipitated calcite is ~0.001 (Hu et al., 2005). A biological influence on groundwater δ^{30}Si values is probably not important for the RI fresh groundwaters because: 1) the area above the freshwater lens is sparsely vegetated due to land clearing and contains no surface water features, and 2) the salt lakes (located to the east of the freshwater lens) that host diatom communities are not hydrologically connected to the groundwater system (Bryan et al., 2016). In contrast, trace elements, such as strontium (Sr) and lithium (Li), are derived mainly from the dissolution of silicate minerals found within carbonate aeolianite matrix of the RI aquifer (Martin et al., 2020). Moreover, these fresh RI groundwaters are saturated with respect to quartz and their Li isotopic compositions suggest that water-rock interactions with secondary minerals occur in the shallow aquifer (Martin et al., 2020). Deeper in the aquifer on RI, there are saline groundwaters that have undergone a greater degree of seawater mixing Bryan et al. (2017). These saline RI groundwaters have lower δ^{7}Li values relative to fresh RI groundwaters, suggesting that they are interacting with the silicate basement rocks (Martin et al., 2020). Here we assess the application of Si isotopes as a weathering proxy in a carbonate-dominated aquifer with well-constrained hydrogeochemical parameters for fresh and saline groundwaters combined with bedrock data. This study presents the first Si isotope measurements in a carbonate island aquifer system and provides insights into subsurface weathering processes on a high spatial resolution scale. We also assess the potential contributions of carbonate-dominated aquifers to the global Si-isotope budget of the oceans.

https://doi.org/10.5194/hess-2020-429
Preprint. Discussion started: 8 October 2020
© Author(s) 2020. CC BY 4.0 License.

2. Study area

The surface features, hydrogeology, climate and geology of Rottnest Island (RI) have been characterised by Bryan et al. (2016, 2017, 2020) and are summarised here. Briefly, RI is a ~19 km^2 island located 18 km from Perth, Australia. The maximum elevation on RI is ~45 m Australian Height Datum (AHD) (Fig. 1). European settlement on RI in the 1830s reduced the native vegetation cover, but revegetation has commenced on the island, except for the area above a freshwater lens located in the central part of the island to increase groundwater recharge there. Sand dunes are a common feature on RI and there is an absence of water courses. There are a number of hypersaline lakes at sea level (Playford and Leech, 1977), and lower-salinity waterbodies in interdunal wetlands on RI (Gouramanis et al., 2012).

The main lithology on RI is the Tamala Limestone, which is a ~115 m thick Late Quaternary carbonate aeolianite that lies unconformably upon Cretaceous fluvial sandstone beds (Playford et al., 1976). The Tamala Limestone deposit on RI forms part of the world's longest (~1,000 km) carbonate aeolianite formation along the western Australian coastline (Brooke, 2001). The silicate content of Tamala Limestone on RI ranges from 1-6 wt.% and mostly comprises quartz sand grains, which is representative of other aeolianites globally (Muhs, 2017). The carbonate minerals present in Tamala Limestone include aragonite, pure calcite, low-Mg calcite, and high-Mg calcite (Martin et al., 2020).

The climate on RI is Mediterranean with hot-dry summers, and mild-wet winters. The annual average rainfall (1880–2015 CE) is 691 mm and annual reference evapotranspiration is 1694 mm, but rainfall on RI has been below average rainfall since the 1960s. The majority of groundwater recharge occurs during large precipitation events in winter. The freshwater lens on RI is located above a ~10 m freshwater-seawater transition zone within the upper section of the Tamala Limestone (Playford et al., 1977). Since the late 1970s, the extent of the freshwater lens has decreased due to a decrease in rainfall, resulting in seawater intrusion into the freshwater lens (Bryan et al., 2016). Sea-level high stands (~2 m higher than present) at ~7 ka (Coshell and Rosen, 1994) and 4.4 ka (Gouramanis et al., 2012) would have probably intruded seawater into the groundwater system.

The studied groundwaters were grouped into three mixing types on the basis of their depth and hydrogeochemical properties: fresh, transition zone 1 (T1), and transition zone 2 (T2) (Table A.1) (Bryan et al., 2017). Fresh groundwaters are shallow (above -1 m AHD), have low TDS values (<1 g L^{-1}), and are expected to be younger (ca. <0.5 ka) with tritium (^{3}H) and radiocarbon ($^{14}C_{DOC}$) values of >0.6 TU and >89 pMC, respectively; moreover, lumped parameter modelling suggests that the mean residence time for fresh groundwaters ranges from ~12 to 36 years (Bryan et al., 2020). In contrast, the T2 groundwaters are the deepest studied here (-5 to -15 m AHD), have higher TDS (7 to 30 g pes on the basis of their depth and hydrogeochemical properties: fresh, transition zone 1 (T1), and transition zone 2 (T2) (Table A.1) (Bryan et al., 2017). Fresh groundwaters are shallow (above -1 m AHD), have low TDS values (<1 g L^{-1}) and are expected to be older (ca. 3-7 ka) with ^{3}H and $^{14}C_{DOC}$ values of <0.3 TU and <67 pMC, respectively. The T1 groundwaters are located at depths between the fresh and T2 groundwaters (-1 to -5 m AHD) and have intermediate compositions due to mixing between fresh and T2 groundwaters caused by seasonal groundwater level fluctuations.

https://doi.org/10.5194/hess-2020-429
Preprint. Discussion started: 8 October 2020
© Author(s) 2020. CC BY 4.0 License.

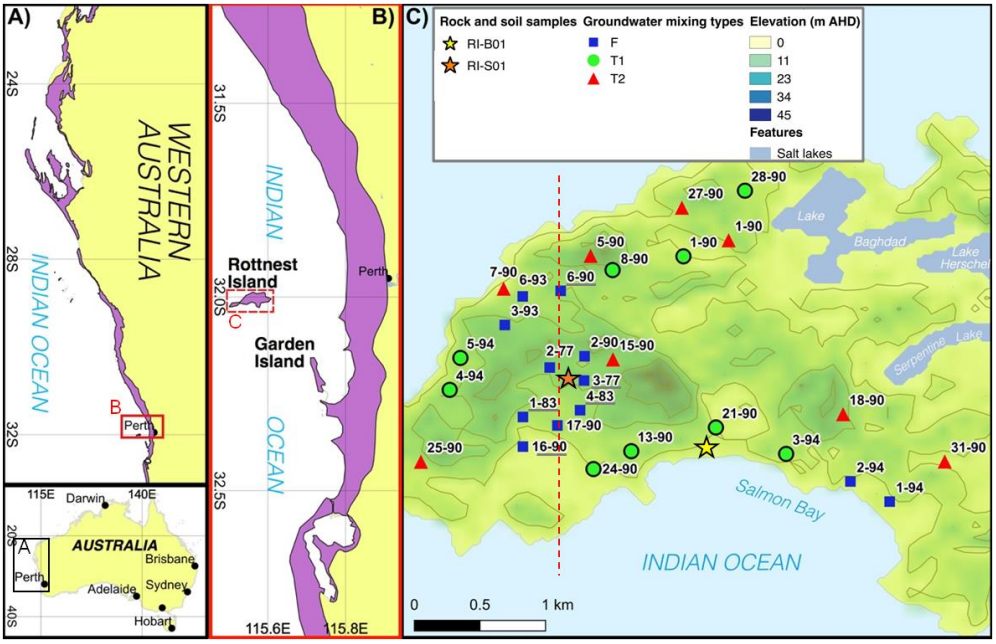

Figure 1. Maps showing the locations of coastal Quaternary deposits in Western Australia (A and B) (Stewart et al., 2008); and C) a Digital Elevation Model of RI, Australia showing sampling locations and IDs (modified from Martin et al., 2020). Groundwater classification types are defined according to Bryan et al. (2017) and underlined sample IDs represent bores with available groundwater residence times modelled by Bryan et al. (2020). The red dashed line in C shows the location of the cross section shown in Fig. 2.

3. Methods

3.1. Sample collection

The groundwater sampling protocols are described in detail by Martin et al. (2020). Briefly, twenty-nine groundwater samples were collected from RI during two field campaigns in September 2014 and March 2015 (Fig. 1). Samples were collected at, or just above the well screen at the bottom of each well (maximum length = 1.5 m). Prior to sample collection, the monitoring and production wells were purged until in-field parameters stabilised . A seawater sample was collected from the shoreline using a peristaltic pump (Masterflex E/S portable sampler).

A rock and soil sample were collected from RI in March 2017. The rock sample (RI-B01) was sampled from an outcrop at Salmon Bay (32°00’46’’S 115°30’33’’E). Only visibly-unweathered material was sampled after removing weathered material using a geological hammer. The soil (RI-S01) was sampled from an unvegetated ridge with an actively-forming dune in the centre of RI, corresponding to the area above the freshwater lens (32°00’19’’S 115°29’48’’E) (Fig. 1).

3.2. Analytical techniques

The concentrations of Si, other major elements, and selected trace elements used in this manuscript were determined by Bryan et al. (2016) and Martin et al. (2020) at the Australian Nuclear Science and Technology Organisation (ANSTO) by ion chromatography and inductively coupled plasma-atomic emission spectroscopy.

Silicon isotope column chromatography procedures were conducted in clean laboratories at ANSTO. Acids used in all procedures were high-purity SEASTAR^{TM} IQ grade hydrochloric acid (HCl) and nitric acid (HNO_3). These were further purified prior to use

https://doi.org/10.5194/hess-2020-429
Preprint. Discussion started: 8 October 2020
© Author(s) 2020. CC BY 4.0 License.

by sub-boiling using Savillex® PFA distillation apparatus and stored in Nalgene® FEP bottles. Dilutions were conducted using >18.2 MΩ (at 25 °C) Milli-Q water. Acid concentrations were determined by titration with sodium hydroxide. Column chromatography was conducted using 1.8 mL Biorad AG 50W-X8 (100–200) cation exchange resin packed in Biorad ® 0.8 x 4 cm polypropylene microcolumns based on the one-step procedure from Georg et al. (2006). Prior to loading samples on columns, the resin and columns were cleaned with 3 mL of 3 M HCl, 6 M HCl, 7 M HNO3, 10 M HCl, 6 M HCl and 3 M HCl (18 mL acid in total) and conditioned with 6 mL of Milli-Q water. An appropriate volume of sample containing 7.2 µg of Si was loaded and eluted using Milli-Q water. Column calibration experiments ensured 100% Si yield, which was accomplished by elution with 4 mL of Milli-Q water. The Si fractions were collected in Savillex® PFA vials, evaporated to incipient dryness on a hotplate at 80°C and then re-dissolved in 2 mL of 2% (v/v) HNO_3. This method yielded samples with a Si concentration of 3.6 ppm for isotopic analysis. Solid samples (RI-B01 and RI-S01), and isotopic reference materials NBS-28 (quartz sand) and IRMM-018a (silica sand) were dissolved by alkali fusion to avoid using hydrofluoric acid. Approximately 10 mg of material was added to a platinum (Pt) crucible and the following reagents were added: 40 mg of $LiBO_2$ (Sigma Aldrich, ACS reagent, >98.0% purity) as a fluxing agent, and 100 mg of $NaNO_3$ (Sigma Aldrich, ReagentPlus®, >99.0%) as an oxidising agent. This mixture was then placed in a pre-heated muffle furnace at 950°C using Pt-clad tongs for 40 min before switching off the furnace and left to cool overnight. The fusion cake was then dissolved in 3 mL of 6 M HNO_3 and transferred to a 50 mL centrifuge tube and diluted to a Si concentration of ~100 ppm. The dissolved reference materials were then processed through the column chemistry in the same manner as for samples.

The intensities of ^{28}, ^{29} and ^{30}Si were analysed by multi-collector inductively-coupled plasma mass spectrometer (MC–ICP-MS) using a Thermo Scientific™ Neptune Plus™ in medium-resolution mode (M/ΔM ≈ 2000) at the Research School of Earth Sciences (RSES), Australian National University (ANU) following the analytical setup of Wille et al. (2010). Briefly, the MC-ICP-MS was operated in dry plasma mode using an ESI-Apex nebulizer with a Telfon inlet system, a demountable torch fitted with an alumina injector and using standard Ni sampler and skimmer cones. Prior to each analytical session, the instrument tuning settings were optimised for signal sensitivity and stability before leaving the instrument stabilise for 2-3 hours prior to commencing sample measurements. An external standard-sample-standard bracketing approach was employed to correct measured isotopic ratios for the mass-dependent sensitivity of Si isotopes during the MC–ICP-MS analyses (Albarède and Beard, 2004). Corrected Si isotopic ratios of samples are presented in ‰ as variations from quartz sand isotopic reference material NBS-28 ($\delta^{30}Si_{NBS\text{-}28}$ = +0.02) where $\delta^{29}Si = [(^{29}Si/^{28}Si)_{sample} / {}^{29}Si/^{28}Si)_{NBS\text{-}28} - 1] \times 1000$ and $\delta^{30}Si = [(^{30}Si/^{28}Si)_{sample} / {}^{30}Si/^{28}Si)_{NBS\text{-}28} - 1] \times 1000$. Silica sand IRMM-018a was analysed as an unknown standard and had a δ^{30}Si value of -1.52 ± 0.12 ‰ (n = 5, 2 s.d.), which is within error to the value measured elsewhere: -1.55 ± 0.25 ‰ (n = 2, 2 s.d.) (Ziegler et al., 2010). A plot of δ^{30}Si vs δ^{29}Si confirms that all samples plot on the mass-dependent fractionation line to yield a fractionation factor (β) of 0.516 ± 0.010 (Fig. A.1). Unfortunately, the uncertainty on β does not permit us to discriminate between kinetic and equilibrium fractionation, which have β values of 0.509 ± 0.000 and 0.518 ± 0.000, respectively (Frings et al., 2016).

4. Results

The DSi concentrations of the RI groundwaters ranged from 64 to 196 µM (Table 1; see Appendix A.2 for geochemical parameters) with an average value of 117 µM. The average value on RI is slightly higher than the average for coastal carbonate aquifers globally (80 ± 63 µM, 1 s.d.; Rahman et al., 2019), but much lower than the average values for other coastal aquifers, e.g. igneous (604 ± 192 µM, 1 s.d.), and 'complex' mixed lithology aquifers (288 ± 245 µM, 1 s.d.; Rahman et al., 2019). The groundwaters on RI were classified as either fresh, T1 or T2-type groundwaters according to their hydrogeochemical properties (Bryan et al., 2017). The TDS values of groundwaters broadly increased with depth for the fresh (<1 g L^{-1}), T1 (1 to 5 g L^{-1}) and

https://doi.org/10.5194/hess-2020-429
Preprint. Discussion started: 8 October 2020
© Author(s) 2020. CC BY 4.0 License.

T2 groundwaters (>5 g L^{-1}) (Fig. 2a). In contrast, there was no correlation between DSi concentrations and depth, or salinity, for the fresh and T1 groundwaters (Fig. 2b), but when adopting a significance level threshold of p = 0.05, the deeper T2 groundwaters exhibited a significant inverse correlation between DSi concentrations and Cl concentrations (ρ = -0.79, p = 0.04, n = 5; Fig. 3a). Moreover, the DSi concentrations of the T1 groundwaters (average: 133 ± 36 µM, 1 s.d.) were higher (p = 0.0002) than those of the fresh groundwaters (average: of 112 ± 23 µM, 1 s.d.) and the T2 groundwaters (average: 107 ± 43 µM, 1 s.d.; p = 0.001) according to Mann-Whitney U tests, which is a non-parametric test suitable for comparing for independent variables with small sample sizes.

The δ^{30}Si values of RI groundwaters ranged from -0.39 to +3.60 ‰ with an average of +1.59 ± 0.89 ‰ (1 s.d., n = 28, Table 1). The δ^{30}Si values in the fresh RI groundwaters (+0.7 to +2.6 ‰) extended to a slightly higher range than those of some continental aquifers (+0.1 to +1.7 ‰; Georg et al., 2009a; Opfergelt et al., 2011), and there was an absence of very low δ^{30}Si values (less than -1.0 ‰), which have been found in some continental aquifers (Georg et al., 2009b; Pogge von Strandmann et al., 2014). The δ^{30}Si values for the shallower fresh (average: +1.26±0.66 ‰, 1 s.d.) and T1 groundwaters (average: +1.27±0.86 ‰, 1 s.d.) could not be distinguished according to a Mann-Whitney U test (p = 0.749), however, the δ^{30}Si values for the deeper T2 groundwaters (average: +2.55±0.60 ‰, 1 s.d.) were resolvably higher than both the fresh groundwaters (p = 0.003), and the T1 groundwaters (p = 0.009). There was a statistically significant correlation between δ^{30}Si values and Cl concentrations for the fresh RI groundwaters (ρ = 0.73, p = 0.008, n = 10), but not for the T1 and T2 groundwaters (ρ = -0.64, p = 0.11, n = 5; Fig. 3b). For the fresh groundwaters, δ^{30}Si values correlated with DSi concentration (ρ = 0.59, p = 0.02, n = 9; Fig. 4a), but this correlation was not found for the T1 or T2 groundwaters (Fig. 4b).

A previous study measured the ^{87}Sr/^{86}Sr ratios and δ^{7}Li values of the RI groundwaters (Martin et al. 2020). These values ranged from 0.709167 to 0.709258 (average: 0.709192, n = 19) and +14.5 ‰ to +36.3 ‰ (average: +29.8 ± 5.9 ‰, 1 s.d., n = 23; see Appendix A.2 for individual values), respectively. No correlations were found between the δ^{30}Si values, ^{87}Sr/^{86}Sr ratios and δ^{7}Li values of the RI groundwaters

The Si concentrations of the rock (RI-B01) and soil (RI-S01) samples were 542 and 839 ppm, respectively), and their δ^{30}Si values were -0.76 and -0.13 ‰, respectively (Table 2). The δ^{30}Si value of RI-S01 is close to the average for the upper continental crust (UCC; -0.25 ± 0.32 ‰, 2 s.d.) (Savage et al., 2013), whereas the value for RI-B01 is slightly below the average UCC value.

https://doi.org/10.5194/hess-2020-429
Preprint. Discussion started: 8 October 2020
© Author(s) 2020. CC BY 4.0 License.

Table 1. DSi concentrations and isotopic ratios and groundwaters and a seawater sample from Rottnest Island

ID	Groundwater type[a]	Sampling Date	Screen Elevation (m AHD)	DSi[b] (µM)	δ^{30}Si (‰)
RI_2-77	F	9/29/14	-0.11	81.9	+0.68
RI_3-77	F	9/29/14	-0.01	89.0	+0.66
RI_1-83	F	9/28/14	0.09	124.6	+1.28
RI_4-83	F	9/30/14	-0.11	113.9	+1.00
RI_2-90	F	9/29/14	-0.50	74.8	+1.24
RI_6-90	F	9/29/14	-0.64	135.3	+2.26
RI_16-90	F	9/28/14	-0.28	138.9	+1.53
RI_17-90	F	9/30/14	0.06	121.1	+1.12
RI_3-93	F	9/29/14	-0.27	117.5	+2.58
RI_6-93	F	9/29/14	-0.22	131.7	+1.61
RI_1-94	F	9/28/14	-0.53	85.5	+0.22
RI_2-94	F	9/28/14	-1.00	128.2	+0.97
RI_1-90	T1	9/29/14	-0.90	128.2	+1.52
RI_8-90	T1	9/29/14	-0.59	192.3	+2.81
RI_7-90	T1	3/12/15	-7.06	NA	NA
RI_13-90	T1	3/11/15	-3.55	NA	+1.24
RI_21-90	T1	9/26/14	-4.04	117.5	+1.44
RI_24-90	T1	9/26/14	-3.47	131.7	+1.22
RI_28-90	T1	9/26/14	-1.52	113.9	-0.39
RI_3-94	T1	9/27/14	-0.72	78.3	+1.79
RI_4-94	T1	9/27/14	-1.83	174.5	+1.23
RI_5-94	T1	9/27/14	-1.87	128.2	+0.61
RI_5-90	T2	9/27/14	-6.90	195.8	+2.63
RI_11-90	T2	9/26/14	-6.19	81.9	+3.60
RI_15-90	T2	9/26/14	-14.92	106.8	+2.74
RI_18-90	T2	9/27/14	-11.16	64.1	+2.80
RI_25-90	T2	9/27/14	NA	99.7	+1.72
RI_27-90	T2	9/26/14	-4.98	113.9	+2.30
RI_31-90	T2	9/28/14	-9.20	85.5	+2.08

[a]Defined by Bryan et al. (2017) (see Table A.1); [b]Measured by Martin et al. (2020).

https://doi.org/10.5194/hess-2020-429
Preprint. Discussion started: 8 October 2020
© Author(s) 2020. CC BY 4.0 License.

Hydrology and Earth System Sciences
Open Access
EGU
Discussions

Table 2. Silicon concentrations, Si isotope ratios, and XRD data[a] for bulk rock samples from Rottnest Island

Sample	Description	Si	δ^{30}Si	Low-Mg Calcite ($[Mg_{0.03}Ca_{0.97}]CO_3$)	High-Mg calcite ($[Mg_{0.129}Ca_{0.871}]CO_3$)	Calcite ($CaCO_3$)	Aragonite ($CaCO_3$)	Quartz (SiO_2)	Sylvine, sodian
		ppm	‰	wt.%	wt.%	wt.%	wt.%	wt.%	wt.%
RI-B01	Rock	542	-0.76	40.7	16.8	26.3	14.7	1.2	0.3
RI-S01	Soil	839	-0.13	28.1	52.7	0	13.2	6.0	0.0

[a]XRD data from Martin et al. (2020).

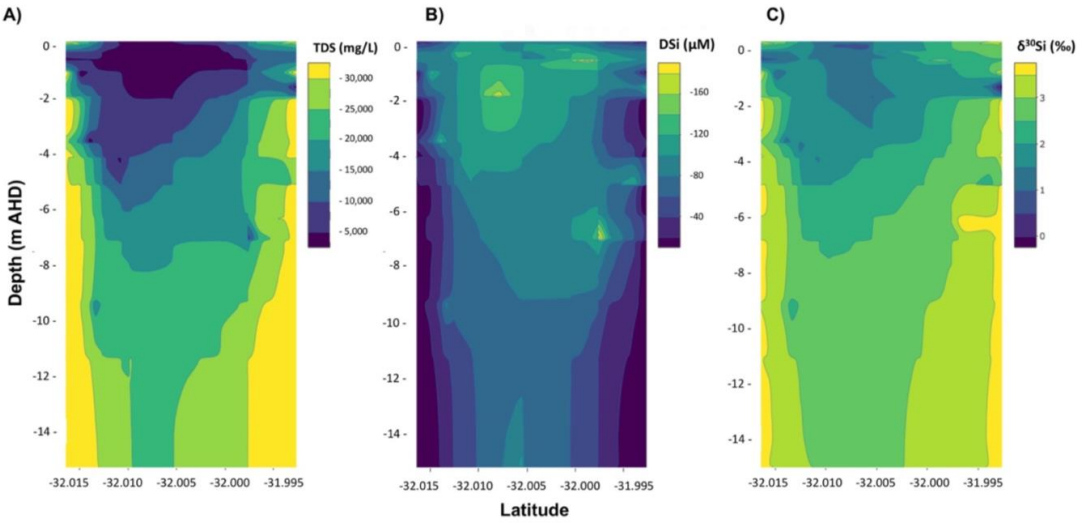

Figure 2. (a) Gridded contour maps for a north-south transect of the aquifer Rottnest Island showing A) TDS values, B) DSi concentrations and C) δ^{30}Si values for groundwaters as a function of depth and latitude in decimal degrees. The grids were created by interpolating groundwater data using the loess function in the base package of the statistical programming language R, which is a non-parametric approach that fits multiple regressions within a given range.

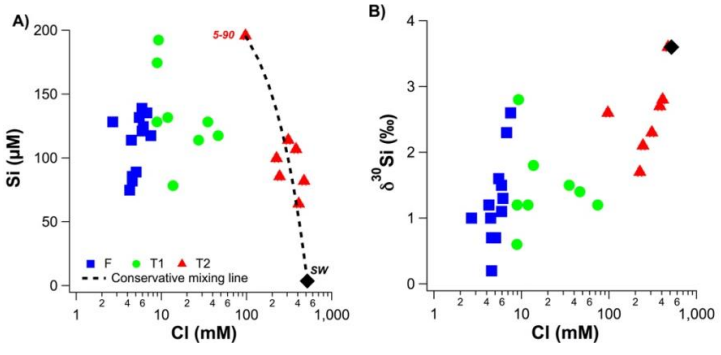

Figure 3. A) Molar DSi concentrations as a function of molar Cl concentrations. B) δ^{30}Si values as a function of molar Cl concentrations. The dashed line in A) represents conservative mixing between local seawater and the T2 groundwater with the highest DSi concentration (well 5-90).

https://doi.org/10.5194/hess-2020-429
Preprint. Discussion started: 8 October 2020
© Author(s) 2020. CC BY 4.0 License.

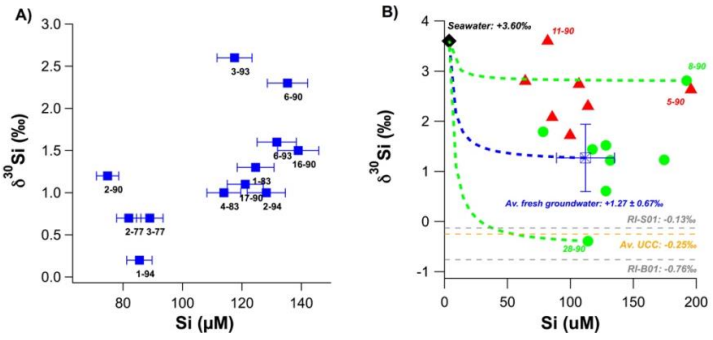

Figure 4. A) Groundwater δ^{30}Si values as a function of molar DSi concentrations for fresh groundwaters; B) Groundwater δ^{30}Si values as a function of molar DSi concentrations T1 (green circles) and T2 groundwaters (red triangles). Dashed lines represent conservative mixing between seawater and the average fresh groundwater (blue dashed line), and seawater and 6-90 (green dashed line). Grey dashed lines show the δ^{30}Si values of RI-S01 and RI-B01 (Table 2). The average δ^{30}Si values for silicate rocks and surface seawater data are from Savage et al. (2013), and Singh et al. (2015). Sample IDs are shown next to markers for all samples in A) and selected samples in B).

5. Discussion

To understand the processes that fractionate Si isotopes in a coastal aquifer, we first attempt to identify the sources of DSi in the unsaturated zone for fresh groundwaters and then consider mechanisms for DSi isotope fractionation. We then consider how the DSi isotope composition of fresh groundwaters evolves in the older and more saline T1 and T2 groundwaters, which are located deeper in the aquifer on RI and have undergone a greater amount of mixing with seawater. Discussion of isotopic compositions is phrased in terms of δ^{30}Si, acknowledging that this is a mass-dependent effect on all Si isotopes.

5.1. Evidence for the source of DSi in fresh groundwaters at Rottnest Island

Dissolution of primary and secondary silicate minerals, i.e., lithogenic silica, appears to be the main process supplying DSi in fresh groundwaters on RI. Assuming that the positive correlation between δ^{30}Si and DSi in fresh groundwaters is caused by water-rock interactions (discussed later in Section 5.2), the regression line between DSi concentration and δ^{30}Si indicates that there is a sole source of DSi with a δ^{30}Si value of -0.68 ± 0.86 (1 s.d.), which lies within the range of δ^{30}Si values (-0.76 to -0.13 ‰; Table 2) measured for the aquifer bedrock (Tamala Limestone). PHREEQC calculations of Martin et al. (2020) using the standard "phreeqc.dat" database (Parkhurst and Appelo, 2013) indicate that all fresh RI groundwaters are saturated with respect to quartz (Table A.2). Thus, we identify the source of DSi as quartz within the Tamala Limestone, which has a quartz content ranging from 1.2 to 6.0 wt.% (Martin et al., 2020). The dissolution of primary silicate minerals, such as quartz, as the main source of DSi has also been recognised in other aquifers (Ehlert et al., 2016;Opfergelt et al., 2011;Georg et al., 2009a). Another possibility is that DSi is supplied from the dissolution of secondary minerals, e.g., clay minerals and silcrete**.** We do not intend to distinguish detrital phases from secondary weathering products produced in-situ, however, if the dissolution of secondary minerals was occurring on RI, lower δ^{30}Si values (less than -1 ‰) would be expected, as measured in the Navajo sandstone aquifer (Georg et al., 2009b) and the mixed sedimentary (alternating layers of sandstone, siltstone and mudstone) Great Artesian Basin, Australia (Pogge von Strandmann et al., 2014). We do not consider that DSi in fresh RI groundwaters is supplied from the dissolution of biogenic silica (BSi), because there is no reported occurrence of biogenic opal in the Tamala Limestone (Semeniuk and Semeniuk, 2006;Hearty and O'Leary, 2008); moreover, BSi is highly reactive and unlikely to be preserved in coastal sediments (Ehlert et al., 2016). Seawater also does not appear to be an important source of DSi in the fresh RI groundwaters due to the low (<1%) estimated

https://doi.org/10.5194/hess-2020-429
Preprint. Discussion started: 8 October 2020
© Author(s) 2020. CC BY 4.0 License.

seawater fractions of the fresh groundwaters (Bryan et al., 2016), and the very low DSi concentrations in seawater (<3.6 μM; Martin et al., 2020), compared to the RI groundwaters (>64 μM; Table 1). The similarly low DSi concentrations in rainfall (<3.6 μM; Martin et al., 2020) also exclude rainfall as an important source of DSi to the groundwaters; moreover, the evaporation of rainfall is not important due to the episodic nature of rainfall events on RI that recharge the aquifer and the resulting low effective rates of evaporation of rainfall (Bryan et al., 2020). Although carbonate minerals are abundant in the Tamala Limestone, they are also not expected to be important sources of DSi to fresh RI groundwaters, which can be demonstrated using data from leaching experiments on the Tamala Limestone by Martin et al. (2020). Leaching of the bulk rock and the overlying soil with 0.5 M HCl showed that the acid-soluble phase had Si/Ca values of 0.11 and 0.05 μM mM^{-1}, respectively. By adopting an upper limit Si/Ca value of 0.11 μM mM^{-1} and using the groundwater Ca concentrations measured by Martin et al. (2020), we estimate that carbonate dissolution contributes <0.18 μM of DSi (<0.2%) to the fresh groundwaters and is, thus, an insignificant component of the DSi budget on RI.

5.2. Evolution of δ^{30}Si values in fresh groundwaters

The increase of δ^{30}Si in fresh groundwaters from +0.22 to +2.26 ‰ relative to DSi concentrations (Fig. 4a) could have occurred by any of the following mechanisms: 1) the incorporation of Si into newly formed clay minerals (Frings et al., 2015;Georg et al., 2007;Hughes et al., 2013;Opfergelt et al., 2017;Pogge von Strandmann et al., 2012), 2) amorphous silica precipitation (Oelze et al., 2015;Geilert et al., 2014;Opfergelt et al., 2017), and 3) the adsorption of Si onto Fe-Al (oxy)hydroxides (Opfergelt et al., 2009;Oelze et al., 2014). Attributing the enrichment in the heavier Si isotopes in fresh RI groundwaters to incongruent weathering during clay mineral formation and/or silica formation would be plausible considering the correlation between DSi concentration and δ^{30}Si (ρ = 0.59, p = 0.02, n = 9; Fig. 4a). However, PHREEQC calculations indicate that fresh RI groundwaters are undersaturated with respect to both aluminosilicate clay minerals and amorphous silica (Table A.2). Undersaturation of clay minerals is explained by the low Al concentrations (<0.3 μM) in fresh RI groundwaters, whereas amorphous silica is very soluble under ambient temperature and pressure conditions and only precipitates at DSi concentrations in excess of 2 mM (Gunnarsson and Arnórsson, 2000), which is an order of magnitude higher than those in fresh RI groundwaters (Table 1). Furthermore, the Al concentrations in fresh RI groundwaters (<0.3 μM) are well below the threshold required for Si isotope fractionation to occur during silica precipitation (~4 μM), which was determined in a series of experiments that found no isotopic fractionation when silica precipitated in the absence of Al (Oelze et al., 2015). Therefore, we attribute the increase in the δ^{30}Si values of fresh RI groundwaters to the adsorption of the lighter Si isotopes onto Fe-Al (oxy)hydroxides, which can bind DSi over a wide range of pH conditions (Fein et al., 2002), and thereby fractionate Si isotopes via kinetic and equilibrium isotope fractionation mechanisms (Oelze et al., 2014;Opfergelt et al., 2009). Supporting evidence for the occurrence of ion-exchange in fresh RI groundwaters include an excess of Mg and a deficit of Na and Ca relative to conservative mixing with seawater (Bryan et al., 2017). In addition, the δ^{7}Li values of fresh RI groundwaters were remarkably high (>23 ‰), indicating that Li is undergoing isotopic fractionation during the adsorption of Li onto secondary phases (Martin et al., 2020). We infer that the source of Fe-Al (oxy)hydroxides in the aquifer are analogous to the 'terra rossa' Late Quaternary paleosol units that occur throughout the Tamala Limestone (Smith et al., 2012;Hearty and O'Leary, 2008), and similar materials could occur distributed through the aquifer rather than being specifically the paleosols themselves. Terra rossa paleosol units formed on RI during Late Quaternary sea-level low stands, which permitted dune stabilisation of the carbonate sands, some degree of soil development and the accumulation of Fe-rich atmospheric dust from the Australian continent (Smith et al., 2012;Hearty and O'Leary, 2008). As paleosol units act as inception horizons in the Tamala Limestone and may define preferential groundwater flow paths through the aquifer (Hearty and O'Leary, 2008), it is likely that groundwaters will flow through or along paleosol units on RI. Moreover, as it has been shown that the enrichment of heavier Si isotopes in the aqueous phase depends on the degree of soil weathering, the Fe-oxide content, and the proportion of short-range

https://doi.org/10.5194/hess-2020-429
Preprint. Discussion started: 8 October 2020
© Author(s) 2020. CC BY 4.0 License.

ordered Fe-oxides (Opfergelt et al., 2009), the extent of Si isotopic fractionation in fresh RI groundwaters may depend on the specific geochemical properties of the paleosol units through which they flow and produce spatial variations in Si isotopic compositions. If this hypothesis is correct, Si isotopic fractionation may not occur by this process in groundwaters draining carbonate lithologies that have undergone a greater degree of karstification, where it might be expected that the paleosol unit has been weathered out.

We also observe a spatial pattern in groundwater δ^{30}Si values across the freshwater lens and propose that this may be explained in terms of the hydrogeology of RI. For instance, the highest δ^{30}Si values are found in the northeastern and northwestern portions of the freshwater lens (wells 6-90 and 3-93). Although these groundwaters are defined as "fresh" in terms of their TDS concentrations (<1 g L^{-1}), there is a greater degree of upward mixing of older, more saline groundwater from the freshwater-seawater transition zone in these wells (Bryan et al., 2020). In contrast, the lowest δ^{30}Si values are found in the central area of the freshwater lens (wells 2-77, 2-90 and 3-77) and SW areas of the freshwater lens (1-94 and 2-94; Fig. 5a). These groundwater wells typically receive more rainfall recharge and have the shortest groundwater residence times according to their ^{3}H activities (Bryan et al., 2020). Thus, groundwater δ^{30}Si values may broadly reflect the degree to which they have undergone mixing with older, more saline groundwaters from the freshwater-seawater transition zone. For example, mixing processes may explain the correlation between the δ^{30}Si values and Cl concentrations of fresh groundwaters (Fig. 3b), and between δ^{30}Si values and ^{3}H activities when considering all groundwater types (Fig. 6). The specific extent of Si isotopic fractionation in groundwaters may depend on the geochemical properties of the paleosol units through which they flow, e.g., Fe-oxide content and mineralogy (Opfergelt et al., 2009). The DSi and Si isotope composition of the T1 groundwaters are discussed in Section 5.3.

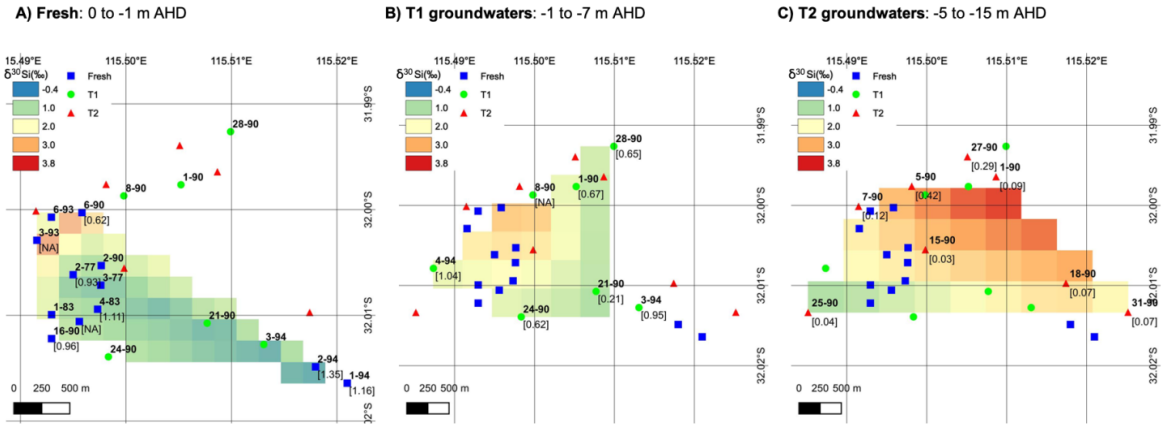

Figure 5 Interpolated spatial plots of δ^{30}Si values for groundwaters at RI for the A) fresh, B) T1 and C) T2 groundwaters. The data were created using a TIN interpolation function (cubic interpolation method) with a pixel size of ca. 0.002 (A) to 0.003° (B and C), depending on sample density per unit area. Sample IDs are shown in bold text next to markers and values in square brackets show ^{3}H values from Bryan et al. (2016).

https://doi.org/10.5194/hess-2020-429
Preprint. Discussion started: 8 October 2020
© Author(s) 2020. CC BY 4.0 License.

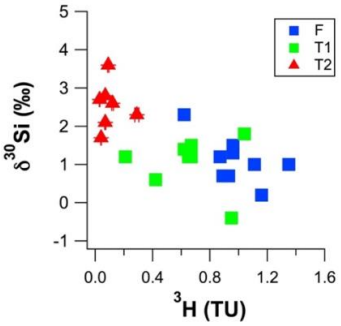

Figure 6 δ^{30}Si values for RI groundwaters as a function of their ^{3}H concentrations (in tritium units; TU)

5.3. Groundwater processes in the freshwater-seawater transition zone

Groundwaters in the freshwater-seawater transition zone on RI can be into two water types on the basis of their chemical and isotopic composition as T1 or T2 groundwaters (Bryan et al., 2017). The T2 groundwaters are the deeper, older, and more saline, whereas the T1 groundwaters have compositions that are dominated by mixing between the fresh and the more saline T2 groundwaters. This mixing is driven by tidal and groundwater level fluctuations within the transition zone and variable meteoric recharge (Bryan et al., 2016). In this section we first assess the evolution of δ^{30}Si values in T1 groundwaters

5.3.1. Evidence for lithogenic silica dissolution in T1 groundwaters

The dissolution of lithogenic silica appears to occur in both the freshwater lens and in the freshwater-seawater transition zone. This is supported by the T1 groundwaters having significantly higher DSi concentrations than both fresh ($p = 0.0002$) and T2 groundwaters ($p = 0.001$, Table 1). Furthermore, the average δ^{30}Si value of fresh and T1 values are statistically identical within the distribution of the data, and most T1 groundwaters lie within one standard deviation of the average δ^{30}Si value for fresh groundwaters (Fig. 4b). Based on these observations, we infer that similar Si isotopic fractionation mechanisms are occurring in fresh and T1 groundwaters whilst DSi concentrations increase. The dissolution of silicate minerals in saline groundwaters has also been observed in a quartz-rich, sandy, barrier island aquifer on Spiekeroog, northern Germany (Ehlert et al., 2016). The two T1 groundwaters collected from wells 8-90 and 28-90 that have the highest and lowest δ^{30}Si values, respectively, do not fit this interpretation. The low δ^{30}Si value well 28-90 (-0.39 ‰, Table 1) could be explained by the dissolution of Tamala Limestone (-0.76 to -0.13 ‰, Table 2) in this groundwater whilst not undergoing secondary mineral formation, or interacting with paleosol units, or any other phases that may preferentially adsorb Si. In contrast, the high δ^{30}Si value for well 8-90 (+2.81 ‰) is associated with the highest DSi concentration of all T1 groundwaters (192 μM) suggesting that, at this location in the freshwater-seawater transition zone, the dissolution of silicate minerals is accompanied by enhanced Si adsorption onto secondary phases. As the T1 groundwaters are undergoing mixing with more saline groundwaters from the deeper aquifer and meteoric groundwaters from the freshwater lens, the δ^{30}Si values of T1 groundwaters may be represented by a three-component end-member mixing model between seawater (low DSi, high δ^{30}Si), groundwaters that have undergone less extensive water-rock interactions (low DSi, low δ^{30}Si, e.g., well 28-90), and groundwaters that have undergone more extensive water-rock interactions (high DSi, high δ^{30}Si, e.g., well 8-90).

https://doi.org/10.5194/hess-2020-429
Preprint. Discussion started: 8 October 2020
© Author(s) 2020. CC BY 4.0 License.

5.3.2. Silicon isotope dynamics of meteoric groundwaters during mixing with seawater

Mixing of seawater with the more saline T2 groundwaters in the deeper aquifer on RI appears to reduce groundwater DSi concentrations. This dilution of the DSi concentrations for the T2 groundwaters can be explained by the low concentration of DSi in local seawater (<3.6 μM; Table 1), and the higher seawater fractions of the T2 groundwaters (>17%; Bryan et al., 2017), as supported by the negative correlation between DSi and Cl (ρ = -0.79, p = 0.04, n = 7). All T2 groundwaters plot broadly on a mixing line between seawater (<3.6 μM DSi) and the well with highest groundwater DSi concentration (well 5-90, Fig. 3a). This suggests that the primary variable controlling the magnitude of DSi concentrations in T2 groundwaters is the extent to which they have undergone conservative mixing with seawater, plus the extent of lithogenic silica dissolution that produced the groundwater endmember with a high DSi concentration. Thus, the extent of variation is controlled by mixing but the absolute DSi concentrations are controlled by the other endmember with high DSi. The secondary control on DSi concentrations in T2 groundwaters may be related to silicate weathering and water-rock interactions, which would also influence their Si isotopic composition, and may explain why the Si isotopic compositions of the T2 groundwaters do not display conservative mixing relationships with seawater (Fig. 4b).

The higher δ^{30}Si values for the deeper T2 groundwaters compared to the fresh and Tl groundwaters may be attributed to groundwater mixing with local seawater that has a low DSi concentration and a high δ^{30}Si value, but there may be evidence for further water-rock interactions. Firstly, the groundwater with the highest seawater fraction (84%, well 11-90) also has the highest δ^{30}Si value (+3.6 ‰, Table 1). This corresponds to the maximum value of a surficial seawater sample from the Bay of Bengal, Indian Ocean, which exhibited a DSi concentration of 6.3 μM (Singh et al., 2015). The inverse relationship between DSi and δ^{30}Si in seawater is well-established and has been explained by the preferential incorporation of lighter Si isotopes by diatoms (Singh et al., 2015;Grasse et al., 2013). However, the correlation between Cl and δ^{30}Si for the T2 groundwaters is weak not statistically significant (ρ = 0.64, p = 0.11, n = 5). If seawater mixing with groundwaters is conservative with respect to Si, the weak correlation between Cl and δ^{30}Si may be explained by a variable initial end-member isotopic composition for the groundwater component, which is likely represented by the T1 groundwaters (Fig. 3a). Alternatively, saline groundwaters may not undergo conservative seawater mixing with respect to DSi due to silicate dissolution and water-rock interactions. Groundwater ^{3}H and ^{14}C data indicate that there is older (>3 ka) seawater 'trapped' under RI in the deeper aquifer (Bryan et al., 2017). Additional evidence for ongoing weathering reactions in the deeper aquifer is the δ^{7}Li value of the T2 groundwater from the deepest well exhibiting the lowest δ^{7}Li value measured on RI (Martin et al., 2020). Thus, the prolonged residence time of deeper groundwaters may increase the extent of water-rock interactions and yield high δ^{30}Si values.

5.4. Implications for the global DSi isotope mass balance

Our conclusion that the dissolution of lithogenic silica is occurring in the freshwater-seawater transition zone supports the inclusion of a 'marine SGD' term in the global DSi mass balance (Rahman et al., 2019;Cho et al., 2018), consistent with the findings from a sand barrier island aquifer in northern Germany (Ehlert et al., 2016). Marine SGD accounts for the marine-derived component of DSi in SGD that is supplied from the lithogenic dissolution of coastal sediments by recirculated seawater. Previous mass balance models only considered terrestrial SGD inputs ('fresh SGD') with a DSi flux of ~0.7 Tmol a^{-1} (Frings et al., 2016;Tréguer and De La Rocha, 2013), which equates to ~10% of the riverine DSi flux. Marine SGD is estimated to supply ~3.1 Tmol a^{-1} of DSi globally (Rahman et al., 2019). The total SGD flux (fresh SGD + marine SGD) is ~3.8 Tmol a^{-1} representing ~60% of the riverine DSi input (~6.3 Tmol a^{-1}) and is six-fold higher than previously recognised. As highlighted by Rahman et al. (2019), the major effect of the revised DSi global mass balance is the large decrease in the estimated DSi oceanic residence time from ~10 to ~8 ka.

https://doi.org/10.5194/hess-2020-429
Preprint. Discussion started: 8 October 2020
© Author(s) 2020. CC BY 4.0 License.

The Si isotopic composition of the marine SGD flux is poorly constrained, and our data provide one of the few direct estimates of this component. This is because RI is a coastal island aquifer that receives no terrestrial runoff and the contribution of DSi from lithogenic silica dissolution in the more saline RI groundwaters can be estimated using our data from the fresh RI groundwaters. As the average δ^{30}Si values for the fresh and T1 groundwaters were similar (+1.26±0.66 ‰ and +1.27±0.86 ‰, respectively; 1 s.d.; Table 1), a value of +1.27 ‰ may be adopted for the marine SGD flux. Adopting this value for the marine SGD flux in a revised DSi mass balance decreases the estimated ocean-average δ^{30}Si value from +0.8 to +0.1 ‰. A value of around +2.6 ‰ for the marine SGD term is required to be consistent with the current estimate of the ocean-average δ^{30}Si value, which corresponds to the δ^{30}Si value of the saline groundwater with the highest DSi concentrations on RI (well 5-90). These estimates are highly uncertain and highlight the need for additional Si isotopic measurements of saline groundwaters to obtain a representative estimate of the marine SGD term and better constrain the global Si isotopic budget.

6. Conclusions

The Si isotopic composition of groundwaters was utilised to trace groundwater processes on RI. The adsorption of Si onto Fe-Al (oxy)hydroxides found in the aquifer rock appears to primarily control δ^{30}Si values in fresh groundwaters on RI. This finding contrasts some other aquifer systems with higher concentrations of DSi and clay-forming cations, e.g. Na and Al, in which Si isotopic fractionation is related to the formation of amorphous silica and aluminosilicate clay minerals. In addition, there was a spatial pattern in groundwater δ^{30}Si values across the freshwater lens. This may be related to the local hydrogeology of RI as higher δ^{30}Si values were found for wells with a greater degree of upward mixing with older, more saline groundwater from the freshwater-seawater transition zone, whereas lower δ^{30}Si values were found in groundwater wells that typically receive more rainfall recharge and have the shortest groundwater residence times. Therefore, the stable Si isotopic composition of groundwaters provides useful information on the degree of water-rock interactions, which is expected to increase with the time elapsed since meteoric recharge.

The main source of DSi in shallow, fresh groundwaters on RI was the dissolution of lithogenic silica found within the carbonate matrix of the aquifer rock. Moreover, this process appears to continue in more saline groundwaters in the freshwater-seawater transition zone, which has been termed the 'marine SGD flux'. Constraining the Si isotopic composition of this flux from key areas, such as volcanic island aquifers, should be a goal of future studies to better constrain the global Si isotopic budget. Although not important on a global scale, the dissolution of lithogenic silica in coastal carbonate aeolianite aquifers may be an important source of oceanic DSi regionally. For instance, the local seawater around RI is depleted in DSi and two orders of magnitude lower than fresh RI groundwaters. Thus, we propose that the coastal carbonate aeolianite aquifers may be an important source of oceanic DSi in other coastal regions with carbonate aquifers where there is no large DSi riverine flux and the oceanic concentration of DSi is low, e.g., The Bahamas or the Yucatán Peninsula, Mexico.

Code and data availability

The data in this manuscript are available from the authors upon request.

Author contribution

AB, KM and MN conceptualised the research. KM and EB collected the water samples, and AM and AB collected the rock and soil samples. AM conducted the analytical work with assistance from MN. AM prepared the manuscript with contributions from all co-authors.

https://doi.org/10.5194/hess-2020-429
Preprint. Discussion started: 8 October 2020
© Author(s) 2020. CC BY 4.0 License.

Competing interests

The authors declare that there are no competing conflicts of interest.

Acknowledgements

The Rottnest Island Authority (RIA) is thanked for supporting this project, especially C. Thomas, L. Wheat and S. Kearney. We also recognise the enduring backing of S. Hollins, Head of Research at ANSTO, in addition to H. Wong and C. Vardanega for supporting ICP-MS and ICP-OES analyses, C. Dimovski and S. Hankin for field trip preparations, and K. Simon and D. Child for usage of the clean laboratory facilities. Les Kinsley at ANU is acknowledged for sharing his wisdom and support in MC-ICPMS analyses. This study was supported by an ARC Linkage grant (LP150100144).

A.1 Appendix

Supporting tables and figures are provided in this Appendix. All geochemical parameters presented in this manuscript are given in Table S1.

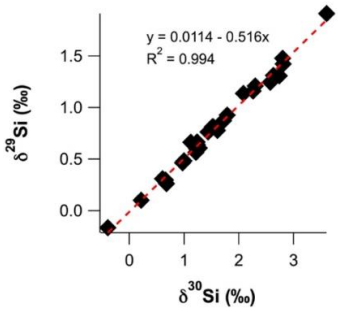

Figure A.1 Linear plot of δ^{29}Si as a function of δ^{30}Si for all groundwater samples

Table A.1 Groundwater mixing types (Bryan et al., 2017)

Mixing type	Depth (m AHD)	TDS (g L^{-1})	^{3}H (TU)	$^{14}C_{DOC}$
Fresh	0 to -1	<1	0.6-1.4	89-105
T1	-1 to -7	1-21	0.2-1.0	84-98
T2	-5 to -15	7-30	0.0-0.3	47-67

Table A.2 Mineral saturation states for fresh groundwaters modelled using PHREEQC3[a]

Phase	X	SI_3-77 (fresh)	SI_2-94 (mature)
Aragonite	$CaCO_3$	-0.12	0.10
Calcite	$CaCO_3$	0.03	0.24
Dolomite	$CaMg(CO_3)_2$	0.29	0.21
Gibbsite	$Al(OH)_3$	-1.56	-1.81
Gypsum	$CaSO_4{:}2H_2O$	-2.04	-2.08

https://doi.org/10.5194/hess-2020-429
Preprint. Discussion started: 8 October 2020
© Author(s) 2020. CC BY 4.0 License.

K-feldspar	$KAlSi_3O_8$	-3.88	-3.85
K-mica	$KAl_3Si_3O_{10}(OH)_2$	-1.44	-1.90
Kaolinite	$Al_2Si_2O_5(OH)_4$	-2.2	-2.47
Silica (amorphous)	SiO_2	-1.26	-1.13
Quartz	SiO_2	0.07	0.18

[a]PHREEQC modelling using the standard "phreeqc.dat" database (Parkhurst and Appelo, 2013)

Table A.3 Groundwater residence times from Bryan et al. (2020) and corresponding Si isotope data

ID	Min (a)	Max (a)	Average (a)	DSi (µM)	δ^{30}Si (‰)
1-83	15.0	61.6	40.9	124.6	1.3
16-90	12.0	64.0	39.4	138.9	1.5
4-83	11.5	52.4	37.4	113.9	1.0
6-90	26.9	63.6	53.3	135.3	2.3
3-77	17.8	64.9	44.8	89	0.7

References

Albarède, F., and Beard, B.: Analytical methods for non-traditional isotopes, Reviews in Mineralogy and Geochemistry, 55, 113-152, 2004.

Basile-Doelsch, I., Meunier, J. D., and Parron, C.: Another continental pool in the terrestrial silicon cycle, Nature, 433, 399, 2005.

Beck, A. J., Charette, M. A., Cochran, J. K., Gonneea, M. E., and Peucker-Ehrenbrink, B.: Dissolved strontium in the subterranean estuary–Implications for the marine strontium isotope budget, Geochimica et Cosmochimica Acta, 117, 33-52, 2013.

Brooke, B.: The distribution of carbonate eolianite, Earth-Science Reviews, 55, 135-164, http://dx.doi.org/10.1016/S0012-8252(01)00054-X, 2001.

Bryan, E., Meredith, K. T., Baker, A., Andersen, M. S., and Post, V. E. A.: Carbon dynamics in a Late Quaternary-age coastal limestone aquifer system undergoing saltwater intrusion, Science of The Total Environment, 607–608, 771-785, https://doi.org/10.1016/j.scitotenv.2017.06.094, 2017.

Bryan, E., Meredith, K. T., Baker, A., Andersen, M. S., Post, V. E., and Treble, P. C.: How water isotopes (18O, 2H, 3H) within an island freshwater lens respond to changes in rainfall, Water research, 170, 115301, 2020.

Cho, H.-M., Kim, G., Kwon, E. Y., Moosdorf, N., Garcia-Orellana, J., and Santos, I. R.: Radium tracing nutrient inputs through submarine groundwater discharge in the global ocean, Scientific reports, 8, 2439, 2018.

Christina, L., Brzezinski, M. A., and DeNiro, M. J.: A first look at the distribution of the stable isotopes of silicon in natural waters, Geochimica et Cosmochimica Acta, 64, 2467-2477, 2000.

De La Rocha, C., Brzezinski, M. A., DeNiro, M., and Shemesh, A.: Silicon-isotope composition of diatoms as an indicator of past oceanic change, Nature, 395, 680, 1998.

Ding, T., Zhou, J., Wan, D., Chen, Z., Wang, C., and Zhang, F.: Silicon isotope fractionation in bamboo and its significance to the biogeochemical cycle of silicon, Geochimica et Cosmochimica Acta, 72, 1381-1395, 2008.

Ehlert, C., Reckhardt, A., Greskowiak, J., Liguori, B. T., Böning, P., Paffrath, R., Brumsack, H.-J., and Pahnke, K.: Transformation of silicon in a sandy beach ecosystem: insights from stable silicon isotopes from fresh and saline groundwaters, Chemical Geology, 440, 207-218, 2016.

Falkowski, P. G., Barber, R. T., and Smetacek, V.: Biogeochemical controls and feedbacks on ocean primary production, Science, 281, 200-206, 1998.

Fein, J. B., Scott, S., and Rivera, N.: The effect of Fe on Si adsorption by Bacillus subtilis cell walls: insights into non-metabolic bacterial precipitation of silicate minerals, Chemical Geology, 182, 265-273, 2002.

Frings, P. J., Clymans, W., Fontorbe, G., Gray, W., Chakrapani, G. J., Conley, D. J., and De La Rocha, C.: Silicate weathering in the Ganges alluvial plain, Earth and Planetary Science Letters, 427, 136-148, http://dx.doi.org/10.1016/j.epsl.2015.06.049, 2015.

Frings, P. J., Clymans, W., Fontorbe, G., Christina, L., and Conley, D. J.: The continental Si cycle and its impact on the ocean Si isotope budget, Chemical Geology, 425, 12-36, 2016.

Geilert, S., Vroon, P. Z., Roerdink, D. L., Van Cappellen, P., and van Bergen, M. J.: Silicon isotope fractionation during abiotic silica precipitation at low temperatures: Inferences from flow-through experiments, Geochimica et Cosmochimica Acta, 142, 95-114, https://doi.org/10.1016/j.gca.2014.07.003, 2014.

Georg, R., West, A., Basu, A., and Halliday, A.: Silicon fluxes and isotope composition of direct groundwater discharge into the Bay of Bengal and the effect on the global ocean silicon isotope budget, Earth and Planetary Science Letters, 283, 67-74, 2009a.

Georg, R., Zhu, C., Reynolds, B., and Halliday, A.: Stable silicon isotopes of groundwater, feldspars, and clay coatings in the Navajo Sandstone aquifer, Black Mesa, Arizona, USA, Geochimica et Cosmochimica Acta, 73, 2229-2241, 2009b.

Georg, R. B., Reynolds, B. C., West, A. J., Burton, K. W., and Halliday, A. N.: Silicon isotope variations accompanying basalt weathering in Iceland, Earth and Planetary Science Letters, 261, 476-490, https://doi.org/10.1016/j.epsl.2007.07.004, 2007.

Grasse, P., Ehlert, C., and Frank, M.: The influence of water mass mixing on the dissolved Si isotope composition in the Eastern Equatorial Pacific, Earth and Planetary Science Letters, 380, 60-71, 2013.

Gunnarsson, I., and Arnórsson, S.: Amorphous silica solubility and the thermodynamic properties of H4SiO 4 in the range of 0 to 350 C at Psat, Geochimica et Cosmochimica Acta, 64, 2295-2307, 2000.

Hearty, P. J., and O'Leary, M. J.: Carbonate eolianites, quartz sands, and Quaternary sea-level cycles, Western Australia: a chronostratigraphic approach, Quaternary Geochronology, 3, 26-55, 2008.

Hu, C., Huang, J., Fang, N., Xie, S., Henderson, G. M., and Cai, Y.: Adsorbed silica in stalagmite carbonate and its relationship to past rainfall, Geochimica et Cosmochimica Acta, 69, 2285-2292, 2005.

Hughes, H., Sondag, F., Santos, R., André, L., and Cardinal, D.: The riverine silicon isotope composition of the Amazon Basin, Geochimica et Cosmochimica Acta, 121, 637-651, 2013.

Martin, A. N., Meredith, K., Norman, M. D., Bryan, E., and Baker, A.: Lithium and strontium isotope dynamics in a carbonate island aquifer, Rottnest Island, Western Australia, Science of The Total Environment, 715, 136906, https://doi.org/10.1016/j.scitotenv.2020.136906, 2020.

Meyerink, S., Ellwood, M. J., Maher, W. A., and Strzepek, R.: Iron Availability Influences Silicon Isotope Fractionation in Two Southern Ocean Diatoms (Proboscia inermis and Eucampia antarctica) and a Coastal Diatom (Thalassiosira pseudonana), Frontiers in Marine Science, 4, 10.3389/fmars.2017.00217, 2017.

Muhs, D. R.: Evaluation of simple geochemical indicators of aeolian sand provenance: Late Quaternary dune fields of North America revisited, Quaternary Science Reviews, 171, 260-296, https://doi.org/10.1016/j.quascirev.2017.07.007, 2017.

Oelze, M., von Blanckenburg, F., Hoellen, D., Dietzel, M., and Bouchez, J.: Si stable isotope fractionation during adsorption and the competition between kinetic and equilibrium isotope fractionation: Implications for weathering systems, Chemical Geology, 380, 161-171, http://dx.doi.org/10.1016/j.chemgeo.2014.04.027, 2014.

Oelze, M., von Blanckenburg, F., Bouchez, J., Hoellen, D., and Dietzel, M.: The effect of Al on Si isotope fractionation investigated by silica precipitation experiments, Chemical geology, 397, 94-105, 2015.

Opfergelt, S., de Bournonville, G., Cardinal, D., André, L., Delstanche, S., and Delvaux, B.: Impact of soil weathering degree on silicon isotopic fractionation during adsorption onto iron oxides in basaltic ash soils, Cameroon, Geochimica et Cosmochimica Acta, 73, 7226-7240, https://doi.org/10.1016/j.gca.2009.09.003, 2009.

Opfergelt, S., Eiriksdottir, E., Burton, K., Einarsson, A., Siebert, C., Gislason, S., and Halliday, A.: Quantifying the impact of freshwater diatom productivity on silicon isotopes and silicon fluxes: Lake Myvatn, Iceland, Earth and Planetary Science Letters, 305, 73-82, 2011.

Opfergelt, S., Williams, H., Cornelis, J.-T., Guicharnaud, R., Georg, R., Siebert, C., Gislason, S., Halliday, A., and Burton, K.: Iron and silicon isotope behaviour accompanying weathering in Icelandic soils, and the implications for iron export from peatlands, Geochimica et Cosmochimica Acta, 217, 273-291, 2017.

Parkhurst, D. L., and Appelo, C.: Description of input and examples for PHREEQC version 3: a computer program for speciation, batch-reaction, one-dimensional transport, and inverse geochemical calculations, US Geological Survey2328-7055, 2013.

Playford, P. E., Low, G., and Cockbain, A. E.: Geology of the Perth Basin, Western Australia, Geological Survey of Western Australia, 1976.

https://doi.org/10.5194/hess-2020-429
Preprint. Discussion started: 8 October 2020
© Author(s) 2020. CC BY 4.0 License.

Playford, P. E., Leech, R., and Kendrick, G. W.: Geology and hydrology of Rottnest Island, Geological Survey of Western Australia, 1977.

Pogge von Strandmann, P. A., Porcelli, D., James, R. H., van Calsteren, P., Schaefer, B., Cartwright, I., Reynolds, B. C., and Burton, K. W.: Chemical weathering processes in the Great Artesian Basin: Evidence from lithium and silicon isotopes, Earth and Planetary Science Letters, 406, 24-36, 2014.

Pogge von Strandmann, P. A. E., Opfergelt, S., Lai, Y.-J., Sigfússon, B., Gislason, S. R., and Burton, K. W.: Lithium, magnesium and silicon isotope behaviour accompanying weathering in a basaltic soil and pore water profile in Iceland, Earth and Planetary Science Letters, 339-340, 11-23, https://doi.org/10.1016/j.epsl.2012.05.035, 2012.

Rahman, S., Aller, R., and Cochran, J.: The missing silica sink: Revisiting the marine sedimentary Si cycle using cosmogenic 32Si, Global Biogeochemical Cycles, 31, 1559-1578, 2017.

Rahman, S., Tamborski, J. J., Charette, M. A., and Cochran, J. K.: Dissolved silica in the subterranean estuary and the impact of submarine groundwater discharge on the global marine silica budget, Marine Chemistry, 208, 29-42, 2019.

Savage, P. S., Georg, R. B., Williams, H. M., and Halliday, A. N.: The silicon isotope composition of the upper continental crust, Geochimica et Cosmochimica Acta, 109, 384-399, https://doi.org/10.1016/j.gca.2013.02.004, 2013.

Semeniuk, V., and Semeniuk, C.: Sedimentary fill of basin wetlands, central Swan Coastal Plain, southwestern Australia. Part 2: distribution of sediment types and their stratigraphy, Journal of the Royal Society of Western Australia, 89, 185, 2006.

Singh, S. P., Singh, S. K., Bhushan, R., and Rai, V. K.: Dissolved silicon and its isotopes in the water column of the Bay of Bengal: Internal cycling versus lateral transport, Geochimica et Cosmochimica Acta, 151, 172-191, 2015.

Smith, A., Massuel, S., Pollock, D., and Dillon, P.: Geohydrology of the Tamala Limestone Formation in the Perth region: Origin and role of secondary porosity, 2012.

Stewart, A., Sweet, I., Needham, R., Raymond, O., Whitaker, A., Liu, S., Phillips, D., Retter, A., Connolly, D., and Stewart, G.: Surface geology of Australia 1: 1,000,000 scale, Western Australia (digital dataset), Geoscience Australia: Canberra, ACT, Australia, 2008.

Tréguer, P., Nelson, D. M., Van Bennekom, A. J., DeMaster, D. J., Leynaert, A., and Queguiner, B.: The silica balance in the world ocean: a reestimate, Science, 268, 375-379, 1995.

Tréguer, P. J., and De La Rocha, C. L.: The world ocean silica cycle, Annual review of marine science, 5, 477-501, 2013.

Wille, M., Sutton, J., Ellwood, M. J., Sambridge, M., Maher, W., Eggins, S., and Kelly, M.: Silicon isotopic fractionation in marine sponges: A new model for understanding silicon isotopic variations in sponges, Earth and Planetary Science Letters, 292, 281-289, 2010.

Zektser, I., and Loaiciga, H. A.: Groundwater fluxes in the global hydrologic cycle: past, present and future, Journal of Hydrology, 144, 405-427, 1993.